crystals

Supplementary Materials: Mono- and Bimetalic Amidoboranes

Rafał Owarzany, Piotr J. Leszczyński , Karol J. Fijalkowski and Wojciech Grochala

Here we gathered some experimentally obtained data reported in papers we cited in the review. We focused on experimental data available in the literature for mono- and bimetallic amidoboranes: FTIR spectroscopy, Raman scattering, ^{11}B NMR spectroscopy and thermal decomposition evolved gas analysis (TGA/DSC/MS). Figures appear in order of citations in the review paper.

S1	**^{11}B NMR: α-LiAB, NaAB**	[18] Xiong, Z.; et al. *Nat. Mater.* **2008**, *7*, 138.
S2	**TPD/DSC: α-LiAB, NaAB**	[18] Xiong, Z.; et al. *Nat. Mater.* **2008**, *7*, 138.
S3	**TPD: $Ca(AB)_2$**	[19] Wu, H.; et al. *J. Am. Chem. Soc.* **2008**, *130*, 14834.
S4	**XRD: NaAB**	[22] Xiong, Z.; et al. *Energy Environ. Sci.* **2008**, *1*, 360.
S5	**TGA/DSC: NaAB**	[23] Fijalkowski, K.J.; Grochala, W. *J. Mater. Chem.* **2009**, *19*, 2043.
S6	**FTIR: NaAB**	[23] Fijalkowski, K.J.; Grochala, W. *J. Mater. Chem.* **2009**, *19*, 2043.
S7	**TGA/DSC: NaAB**	[24] Fijalkowski, K.J.; et al. *Phys. Chem. Chem. Phys.* **2012**, *14*, 5778.
S8	**FTIR: $LiNa(AB)_2$**	[24] Fijalkowski, K.J.; et al. *Phys. Chem. Chem. Phys.* **2012**, *14*, 5778.
S9	**DSC/IGA: KAB**	[25] Diyabalanage, H.V.K.; et al. *J. Am. Chem. Soc.* **2010**, *132*, 11836.
S10	**Raman: MAB, M=Li–Cs**	[26] Owarzany, R.; et al. *in preparation,* **2016**
S11	**DSC/TG: $AB/0.5MgH_2$**	[28] Kang, X.; et al. *Phys. Chem. Chem. Phys*. **2009**, *11*, 2507.
S12	**Raman: $AB/0.5MgH_2$**	[28] Kang, X.; et al. *Phys. Chem. Chem. Phys*. **2009**, *11*, 2507.
S13	**FTIR: $Mg(AB)_2$**	[29] Luo, J.; et al. *Energy Environ. Sci*. **2012**, *6*, 1018.
S14	**TG/DSC/MS: $Mg(AB)_2$**	[29] Luo, J.; et al. *Energy Environ. Sci*. **2012**, *6*, 1018
S15	**TG: $Ca(AB)_2$**	[31] Diyabalanage, H.V.K.; et al. *Angew. Chem.* **2007**, *46*, 8995.
S16	**^{11}B NMR: $Ca(AB)_2$**	[32] Spielmann J.; et al. *Angew. Chem. Int. Ed.* **2008**, *47*, 6290.
S17	**TG: $Sr(AB)_2$**	[33] Zhang, Q.; et al. *J. Phys. Chem. C* **2010**, *114*, 1709.
S18	**TG: $Sr(AB)_2$**	[33] Zhang, Q.; et al. *J. Phys. Chem. C* **2010**, *114*, 1709.
S19	**FTIR: $Zn(AB)_2$**	[34] Owarzany, R. B.Sc. Thesis, University of Warsaw, **2013**.
S20	**TG: $Al(AB)_3$**	[35] Hawthorne, M.F.; et al. *Final Report*, Uni. of Missouri, **2010**.
S21	**TGA/DSC: $Y(AB)_3$**	[38] Genova, R.V.; et al. *J. Alloys. Comp.* **2010**, *499*, 144.
S22	**FTIR: $Y(AB)_3$**	[38] Genova, R.V.; et al. *J. Alloys. Comp.* **2010**, *499*, 144.
S23	**FTIR: $LiNa(AB)_2$**	[39] Fijalkowski, K.J.; et al. *Dalton Trans.* **2010**, *40*, 4407.
S24	**TGA/DSC: $LiNa(AB)_2$**	[39] Fijalkowski, K.J.; et al. *Dalton Trans.* **2010**, *40*, 4407.
S25	**FTIR: $LiAl(AB)_4$**	[40] Xia, G.; et al. *J. Mater. Chem. A.* **2013**, *1*, 1810.
S26	**MS: $LiAl(AB)_4$**	[40] Xia, G.; et al. *J. Mater. Chem. A.* **2013**, *1*, 1810.
S27	**FTIR: $NaAl(AB)_4$**	[41] Dovgaliuk, I.; et al. *Chem. Eur. J.* **2015**, *21*, 14562.
S28	**TGA/DSC: $NaAl(AB)_4$**	[41] Dovgaliuk, I.; et al. *Chem. Eur. J.* **2015**, *21*, 14562.
S29	**TGA/DSC: $NaMg(AB)_3$**	[42] Kang, X.; et al. *Dalton Trans.* **2011**, *40*, 3799.
S30	**TGA: $Na_2Mg(AB)_4$**	[44] Wu, H.; et al. *Chem. Commun.* **2011**, *47*, 4102.
S31	**FTIR: $M_2Mg(AB)_4$**, M=Na,K	[45] Chua, Y.S.; et al. *Chem. Mater.* **2012**, *24*, 3574.
S32	**TGA: $M_2Mg(AB)_4$**, M=Na,K	[45] Chua, Y.S.; et al. *Chem. Mater.* **2012**, *24*, 3574.

S1. Solid State ^{11}B NMR Spectra of LiAB and NaAB according to:

[18] Xiong, Z.; Yong, C.K.; Wu, G.; Chen, P.; Shaw, W.; Karkamkar, A.; Autrey, T.; Jones, M.O.; Johnson, S.R.; Edwards, P.P.; et al. High-capacity hydrogen storage in lithium and sodium amidoboranes. *Nat. Mater.* **2008**, *7*, 138.

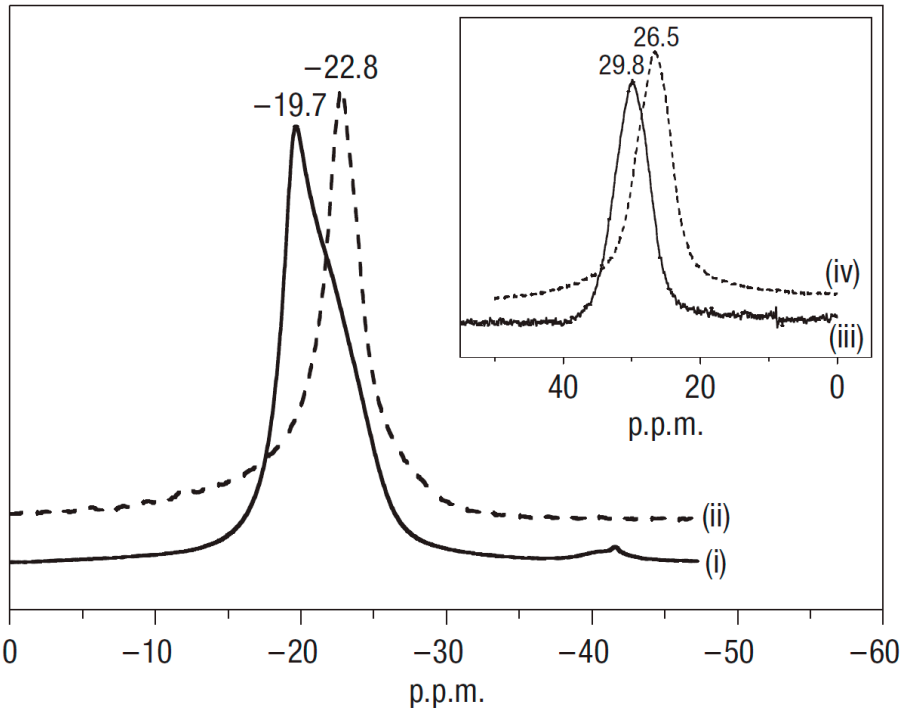

Figure S2. High-field 289.2 MHz (21.2 T) 11B NMR of $LiNH_2BH_3$ and NH_3BH_3 samples. (**i**), As-prepared $LiNH_2BH_3$ sample (−19.7) p.p.m.; (**ii**), untreated NH3BH3 (−22.8 p.p.m.); (**iii**), $LiNH_2BH_3$ sample after dehydrogenation to 140 °C (+29.8 p.p.m.); (**iv**), polyborazylene (+26.5 p.p.m.).

Reproduced from Reference 18 with permission from Nature Publishing Group.

S2. Thermal Decomposition of NaAB according to:

[18] Xiong, Z.; Yong, C.K.; Wu, G.; Chen, P.; Shaw, W.; Karkamkar, A.; Autrey, T.; Jones, M.O.; Johnson, S.R.; Edwards, P.P.; et al. High-capacity hydrogen storage in lithium and sodium amidoboranes. *Nat. Mater.* **2008**, *7*, 138.

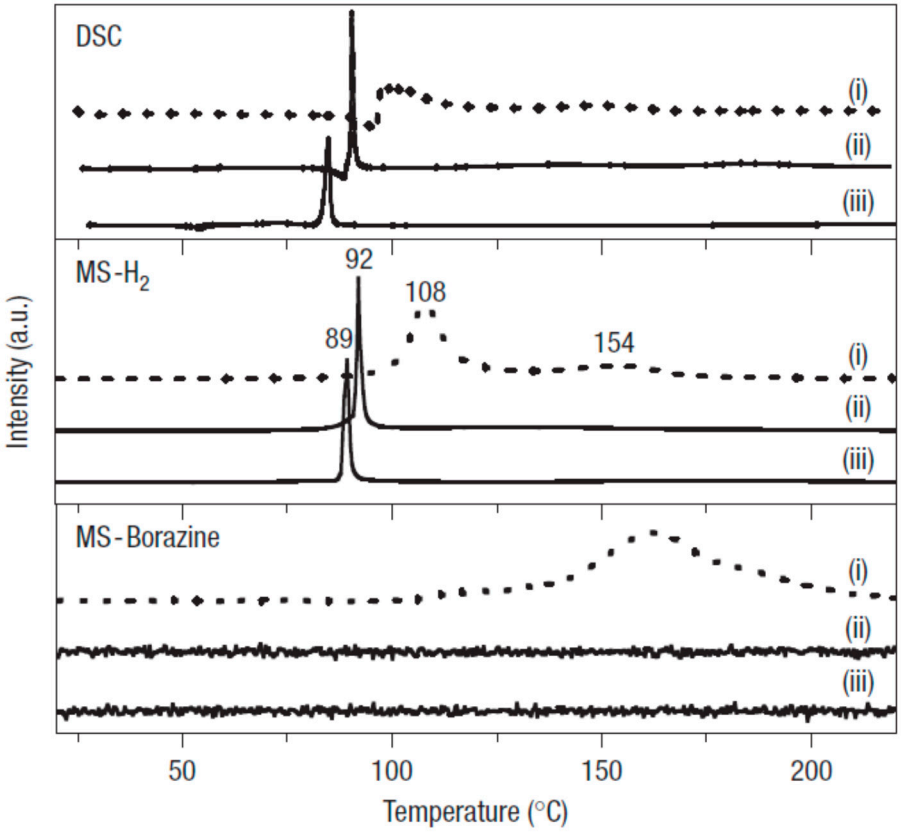

Figure 3. TPD and DSC spectra. (**i**), Post-milled ammonia borane; (**ii**), Li amidoborane sample; (**iii**) Na amidoborane sample. MS: mass spectrometry.

Reproduced from Reference 18 with permission from Nature Publishing Group.

S3. Thermal Decomposition of $Ca(AB)_2$ according to:

[19] Wu, H.; Zhou, W.; Ylidirim, T. Alkali and Alkaline-Earth Metal Amidoboranes: Structure, Crystal Chemistry, and Hydrogen Storage Properties. *J. Am. Chem. Soc.* **2008**, *130*, 14834.

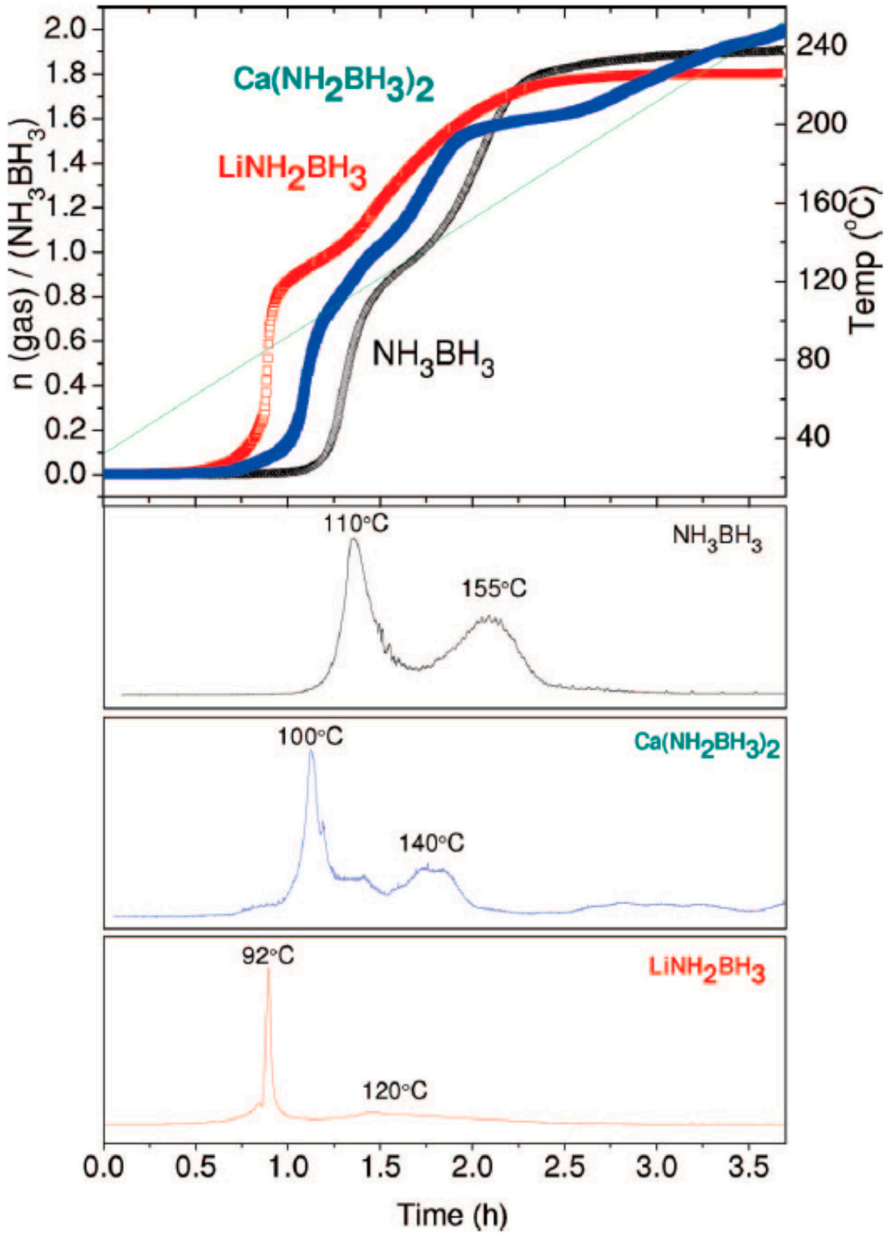

Figure 3. TPD results of hydrogen release for $LiNH_2BH_3$, $Ca(NH_2BH_3)_2$, and NH_3BH_3 with a 1 °C/min heating ramp. Dehydrogenation of $LiNH_2BH_3$ and $Ca(NH_2BH_3)_2$ begins at lower temperatures than NH_3BH_3. The amount of hydrogen gas released has been normalized as n(H_2 gas)/mol of NH_3BH_3.

S4. X-ray Pattern of NaAB according to:

[22] Xiong, Z.; Wu, G.; Chua, Y.S.; Hu, J.; He, T.; Xu, W.; Chen, P. Synthesis of sodium amidoborane ($NaNH_2BH_3$) for hydrogen production. *Energy Environ. Sci.* **2008**, *1*, 360.

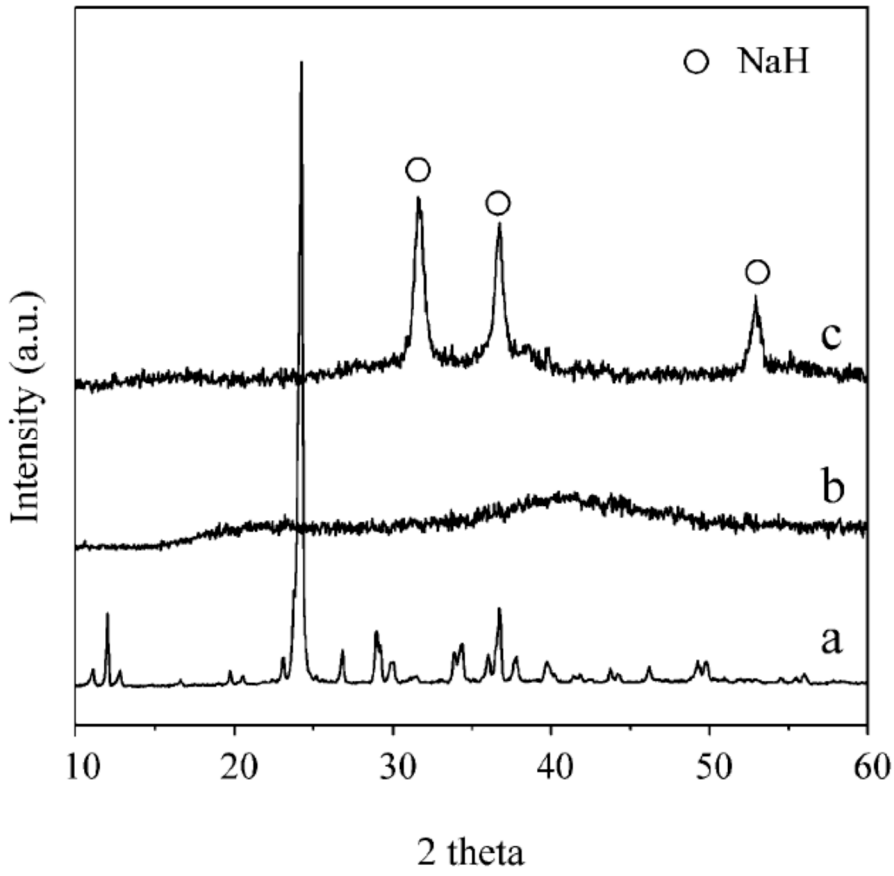

Figure 4. XRD patterns of (**a**) synthesized $NaNH_2BH_3$ and its dehydrogenation product collected at (**b**) 90 °C; (**c**) 200 °C.

Reproduced from Reference 22 with permission from The Royal Society of Chemistry.

S5. Thermal Decomposition of NaAB according to:

[23] Fijalkowski, K.J.; Grochala, W.; Substantial emission of NH_3 during thermal decomposition of sodium amidoborane, $NaNH_2BH_3$. *J. Mater. Chem.* **2009**, *19*, 2043.

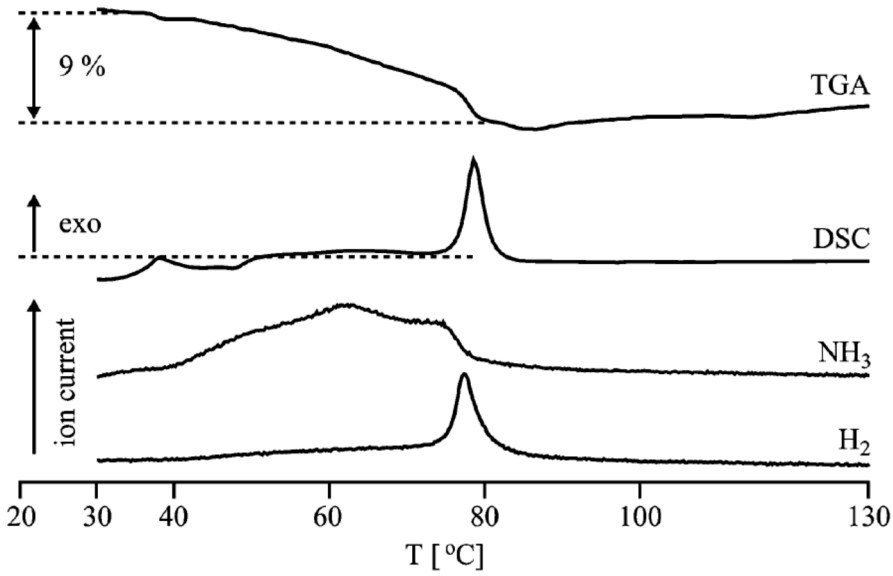

Figure 4. Thermal decomposition of $NaNH_2BH_3$ at 1 °C·min^{-1}: TGA profile (**top**), DSC profile, NH_3 ion current and H_2 ion current (**bottom**).

Reproduced from Reference 23 with permission from The Royal Society of Chemistry.

S6. FTIR Spectra of NaAB according to:

[23] Fijalkowski, K.J.; Grochala, W. Substantial emission of NH_3 during thermal decomposition of sodium amidoborane, $NaNH_2BH_3$. *J. Mater. Chem.* **2009**, *19*, 2043.

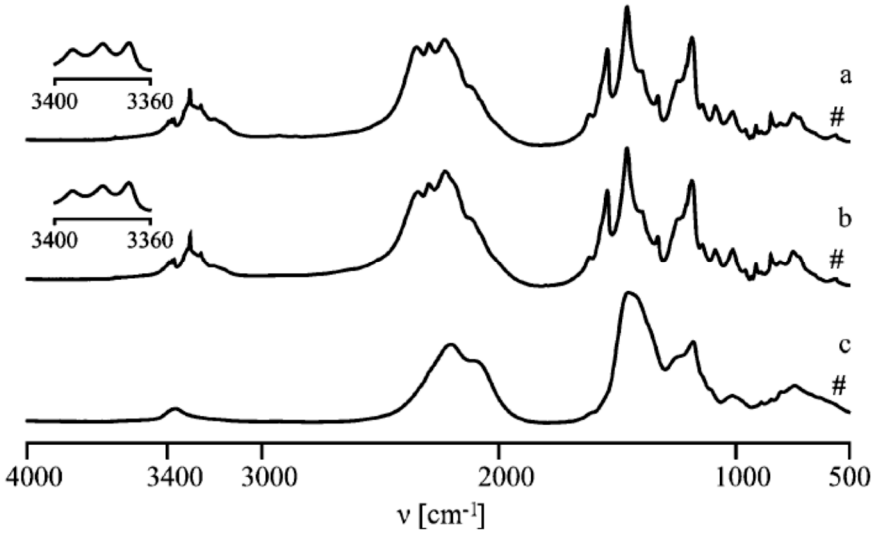

Figure 7. FTIR spectra of SAB containing some NaH (#): (**a**) as-synthesized (25 °C); (**b**) heated to 55 °C; (**c**) heated to 110 °C.

Reproduced from Reference 23 with permission from The Royal Society of Chemistry.

S7. Thermal Decomposition of NaAB according to:

[24] Fijalkowski, K.J.; Jurczakowski, R.; Kozminski, W.; Grochala, W. Insights from impedance spectroscopy into the mechanism of thermal decomposition of $M(NH_2BH_3)$, M = H, Li, Na, $Li_{0.5}Na_{0.5}$, hydrogen stores. *Phys. Chem. Chem. Phys.* **2012**, *14*, 5778.

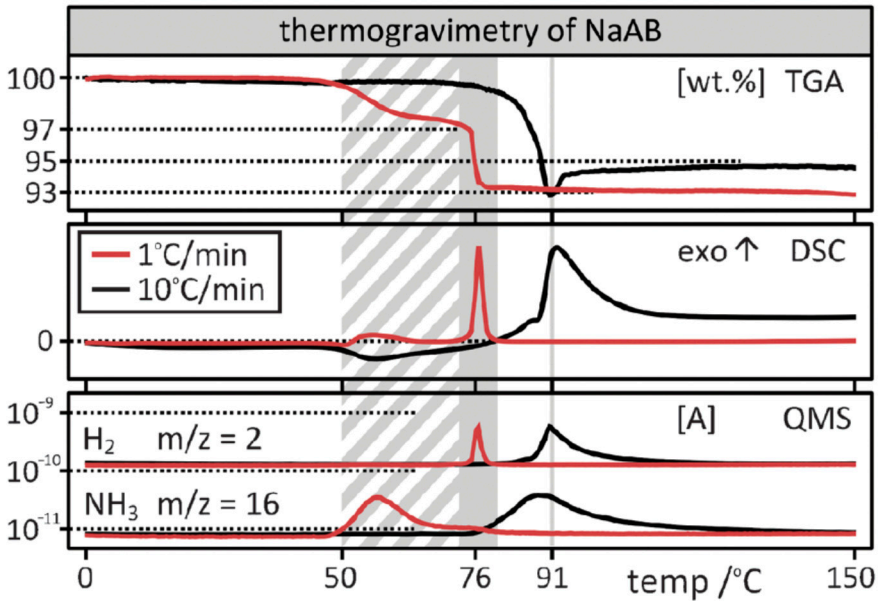

Figure 6. Thermal decomposition of NaAB at 10 K·min^{-1} (black line) and 1 K·min^{-1} (**red line**): TGA profiles (**top**); DSC profiles (**centre**); H_2 and NH_3 ion current (**bottom**). H_2 evolution step at 1 K·min^{-1} is marked with a solid grey field while the NH_3 evolution step with a striped grey field (1·K min^{-1} data).

Reproduced from Reference 24 with permission from the PCCP Owner Societies.

S8. FTIR Spectra of $LiNa(AB)_2$ according to:

[24] Fijalkowski, K.J.; Jurczakowski, R.; Kozminski, W.; Grochala, W. Insights from impedance spectroscopy into the mechanism of thermal decomposition of $M(NH_2BH_3)$, M = H, Li, Na, $Li_{0.5}Na_{0.5}$, hydrogen stores. *Phys. Chem. Chem. Phys.* **2012**, *14*, 5778.

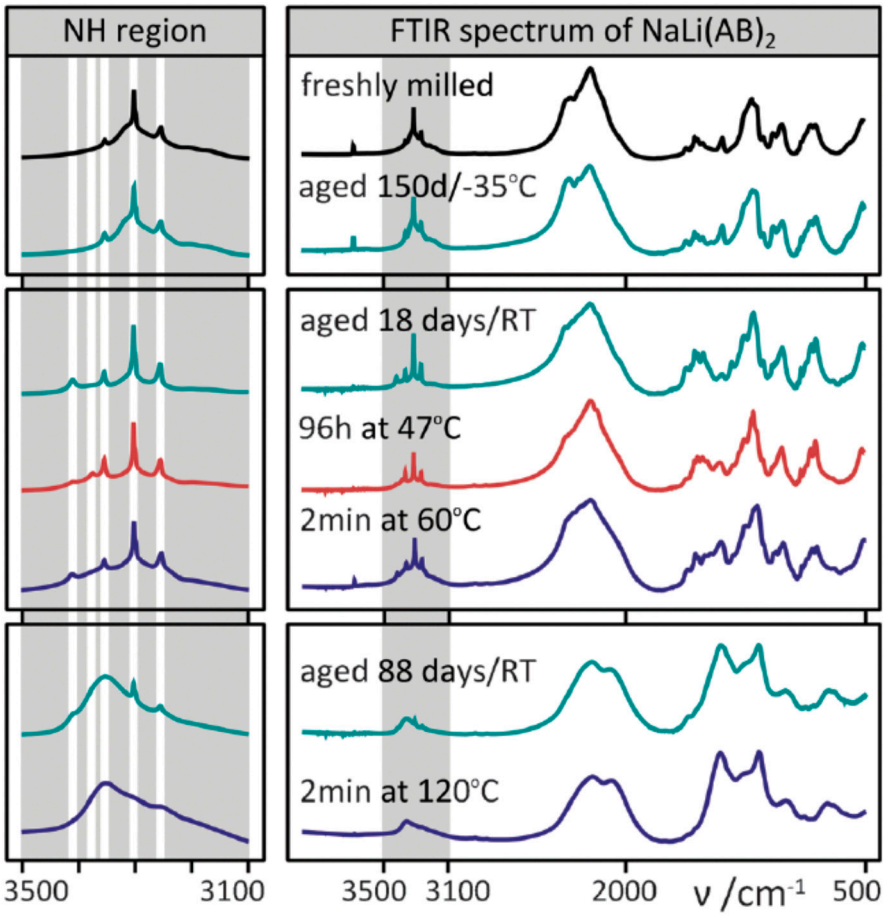

Figure 8. Comparison of FTIR spectra of $NaLi(AB)_2$ under various conditions: a freshly prepared sample and kept at –35 °C (**top**); samples kept at temperatures not exceeding 65 °C or aged at room temperature for less than three weeks (**center**); samples heated above 110 °C and quenched or aged for more than 2 months at room temperature (**bottom**). The diagnostic NH region marked in grey is shown magnified on the left hand side.

Reproduced from Reference 24 with permission from the PCCP Owner Societies.

S9. Thermal Decomposition of KAB according to:

[25] Diyabalanage, H.V.K.; Nakagawa, T.; Shrestha, R.P.; Semelsberger, T.A.; Davis, B.L.; Scott, B.L.; Burrell, A.K.; David, W.I.F.; Ryan, K.R.; Jones, M.O.; et al. Potassium(I) Amidotrihydroborate: Structure and Hydrogen Release. *J. Am. Chem. Soc.* **2010**, *132*, 11836.

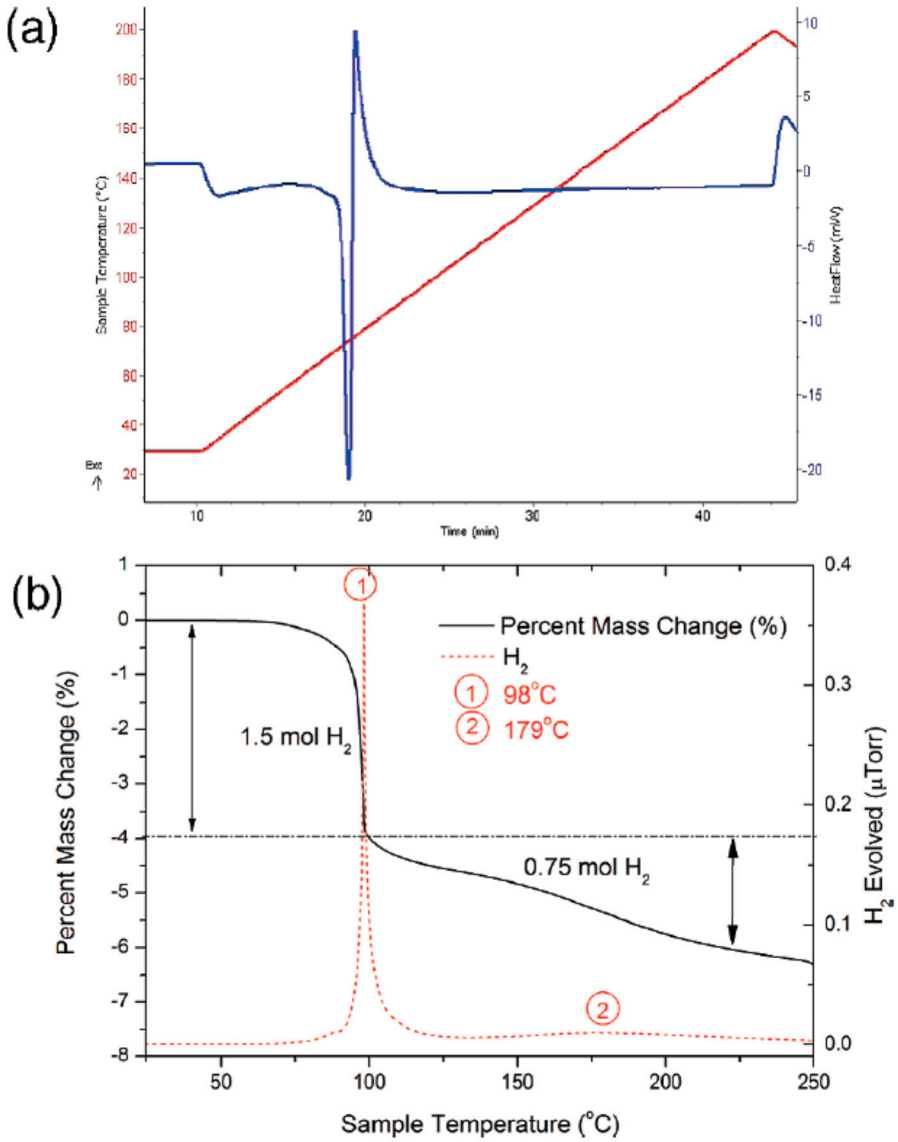

Figure 2. (**a**) DSC and (**b**) IGA data for KNH_2BH_3.

Reprinted with permission from Diyabalanage H.V.K. et al. *J. Am. Chem. Soc.* 2010, 132, 11836. Copyright 2010 American Chemical Society.

S10. Raman spectra of LiAB, NaAB, KAB, RbAB, CsAB according to:

[26] Owarzany, R.; Fijalkowski, K.J.; Palasyuk, T.; Jaroń, T.; Grochala, W. Heavy alkali metal amidoboranes: $RbNH_2BH_3$ and $CsNH_2BH_3$. *In preparation* (**2016**).

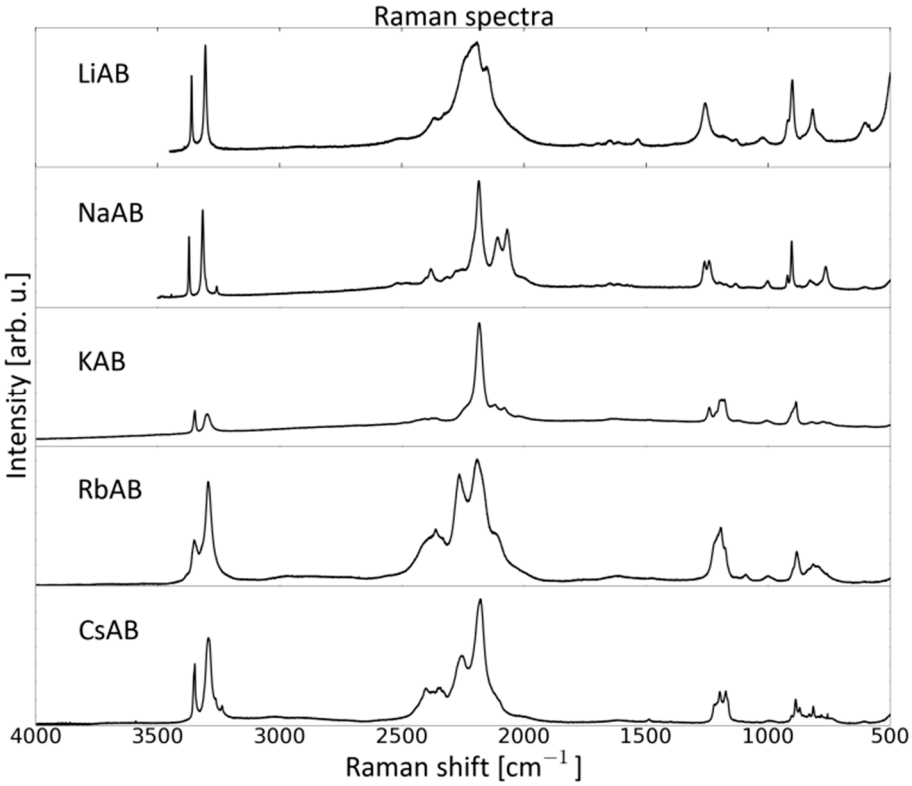

Figure 3. Comparison of Raman scattering spectra of all alkali metal amidoboranes: LiAB, NaAB, KAB, RbAB and CsAB.

Reproduced from Reference 26. With permission of the authors.

S11. Thermal Decomposition of AB/0.5MgH$_2$ according to:

[28] Kang, X.; Ma, L.; Fang, Z.; Gao, L.; Luo, J.; Wang, S.; Wang, P. Promoted hydrogen release from ammonia borane by mechanically milling with magnesium hydride: A new destabilizing approach. *Phys. Chem. Chem. Phys.* **2009**, *11*, 2507.

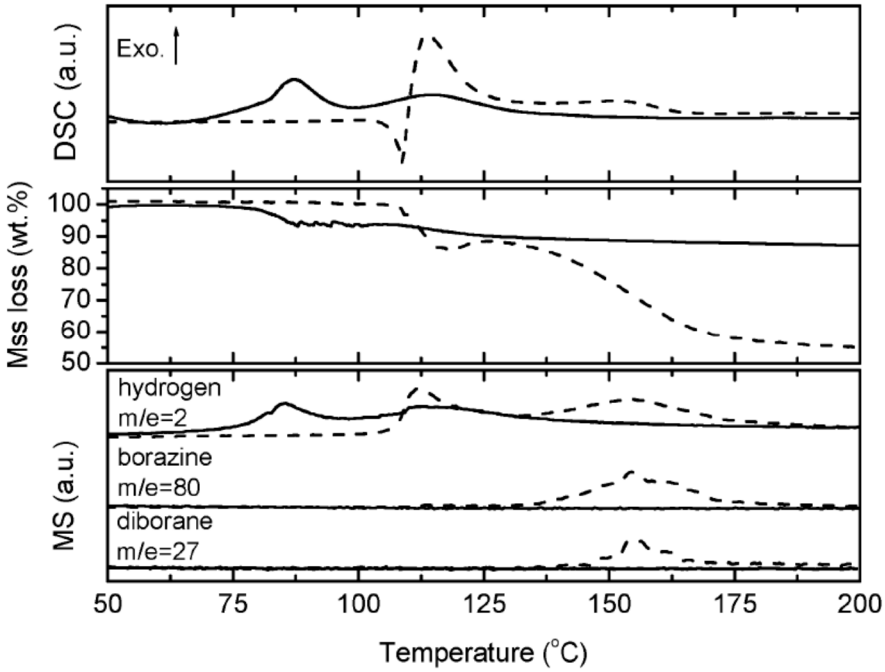

Figure 1. DSC/TG profiles of the post-milled AB/0.5MgH$_2$ (**solid lines**) and neat AB (**dash lines**), and the synchronous MS profiles of m/z = 2 (H_2), m/z = 27 (diborane, B_2H_6), and m/z = 80 (borazine, c-$(NHBH)_3$). The ramping rate is 2 °C·min^{-1}.

Reproduced from Reference 28 with permission from the PCCP Owner Societies.

S12. Raman Spectra of AB/0.5MgH2 according to:

[28] Kang, X.; Ma, L.; Fang, Z.; Gao, L.; Luo, J.; Wang, S.; Wang, P. Promoted hydrogen release from ammonia borane by mechanically milling with magnesium hydride: A new destabilizing approach. *Phys. Chem. Chem. Phys.* **2009**, *11*, 2507.

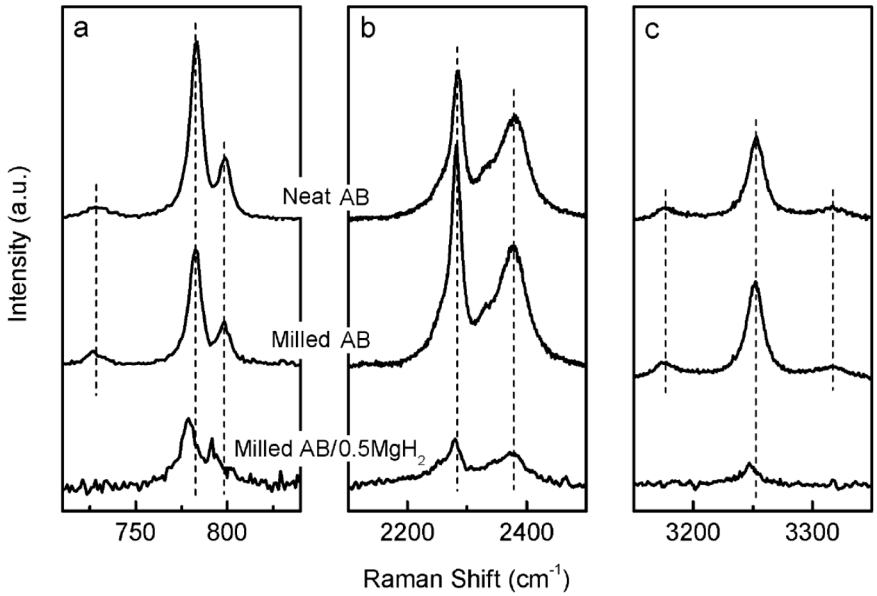

Figure 5. Raman spectra of the milled AB/0.5MgH2, milled AB and neat AB. (**a**) B–N stretching modes; (**b**) B–H stretching modes; and (**c**) N–H stretching modes. The dashed lines were added for guide of eyes.

Reproduced from Reference 28 with permission from the PCCP Owner Societies.

S13. FTIR Spectra of $Mg(AB)_2$ according to:

[29] Luo, J.; Kang, X.; Wang, P. Synthesis, formation mechanism, and dehydrogenation properties of the long-sought $Mg(NH_2BH_3)_2$ compound. *Energy Environ. Sci.* **2013**, *6*, 1018.

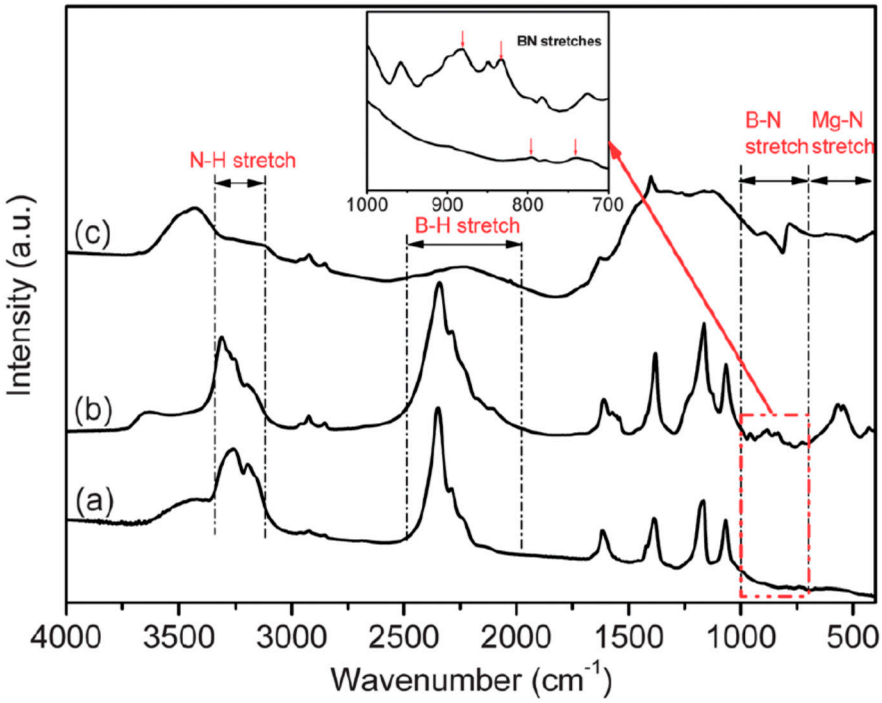

Figure 4. FTIR spectra of (**a**) the post-milled 2AB/Mg sample; (**b**) the aged 2AB/Mg sample with a weight loss of 2.9 wt% (MgAB); and (**c**) the dehydrogenation product(s) of MgAB at 300 °C. The inset shows an enlarged view of the FTIR spectrum of the post-milled and the aged 2AB/Mg samples at a wavenumber range of 1000–700 cm^{-1} and the arrows in the inset were added to indicate the main BN stretches.

Reproduced from Reference 29 with permission from The Royal Society of Chemistry.

S14. TG/DSC/MS spectra of $Mg(AB)_2$ according to:

[29] Luo, J.; Kang, X.; Wang, P.; Synthesis, formation mechanism, and dehydrogenation properties of the long-sought $Mg(NH_2BH_3)_2$ compound. *Energy Environ. Sci.* **2012**, *6*, 1018.

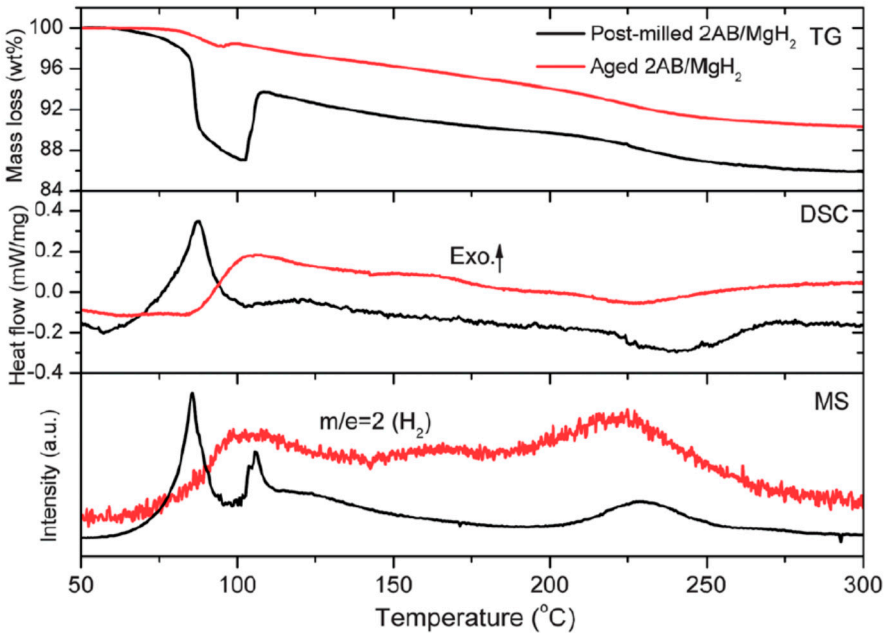

Figure 8. Comparison of the TG/DSC/MS profiles of the post-milled $2AB/MgH_2$ sample and the $2AB/MgH_2$-converted MgAB sample. The fluctuation of the TG profile and the sharp MS signal at around 105 °C in the post-milled 2AB/MgH2 sample resulted from sample foaming, as elaborated in reference 19.

S15. Thermal decomposition of $Ca(AB)_2$ according to:

[31] Diyabalanage, H.V.K.; Shrestha, R.P.; Semelsberger, T.A.; Scott, B.L.; Bowden, M.E.; Davis, B.L.; Burrell, A.K. Calcium Amidotrihydroborate: A Hydrogen Storage Material. *Angew. Chem. Int. Ed.* **2007**, *46*, 8995.

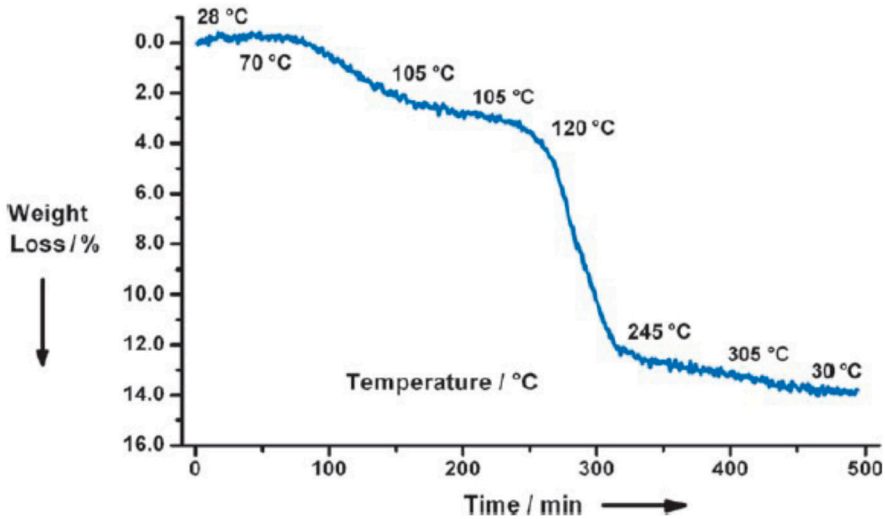

Figure 2. Thermogravimetric analysis of 1; initial loss of THF begins at 70 °C. THF loss is also accompanied by a small release of H_2 before the major hydrogen release begins at 120 °C.

Reproduced from Reference 31 with permission from John Wiley and Sons.

S16. ^{11}B NMR Spectra of Ca(AB)$_2$ according to:

[32] Spielmann, J.; Jansen, G.; Bandmann, H.; Harder, S. Calcium Amidoborane Hydrogen Storage Materials: Crystal Structures of Decomposition Products. *Angew. Chem. Int. Ed.* **2008**, *47*, 6290.

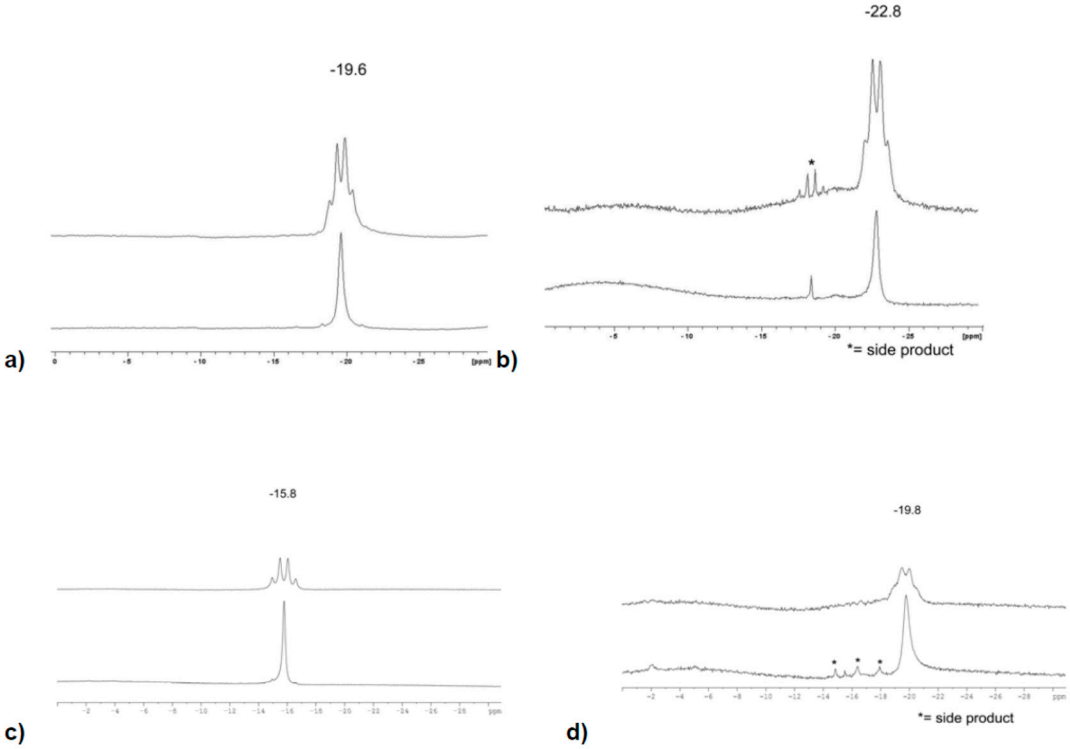

SI: Figure 9. 11B spectra (160 MHz, 20 °C) 1H coupled and decoupled (GARP) (**a**) (DIPP-nacnac)CaNH2BH3·thf [toluene-d8]; (**b**) [(DIPPnacnac)Ca·thf]2[HN-B(H)-N(H)-BH3] [toluene-d8]; (**c**) (DIPP-nacnac)Ca(MeNHBH3)·thf [C6D6], (**d**) [(DIPP-nacnac)Ca·(thf)0.5]2[MeN-B(H)-N(Me)-BH3] [C6D6].

S17. Thermal Decomposition of $Sr(AB)_2$ according to:

[33] Zhang, Q.; Tang, C.; Fang, C.; Fang, F.; Sun, D.; Ouyang, L.; Zhu, M. Synthesis, Crystal Structure, and Thermal Decomposition of Strontium Amidoborane. *J. Phys. Chem. C* **2010**, *114*, 1709.

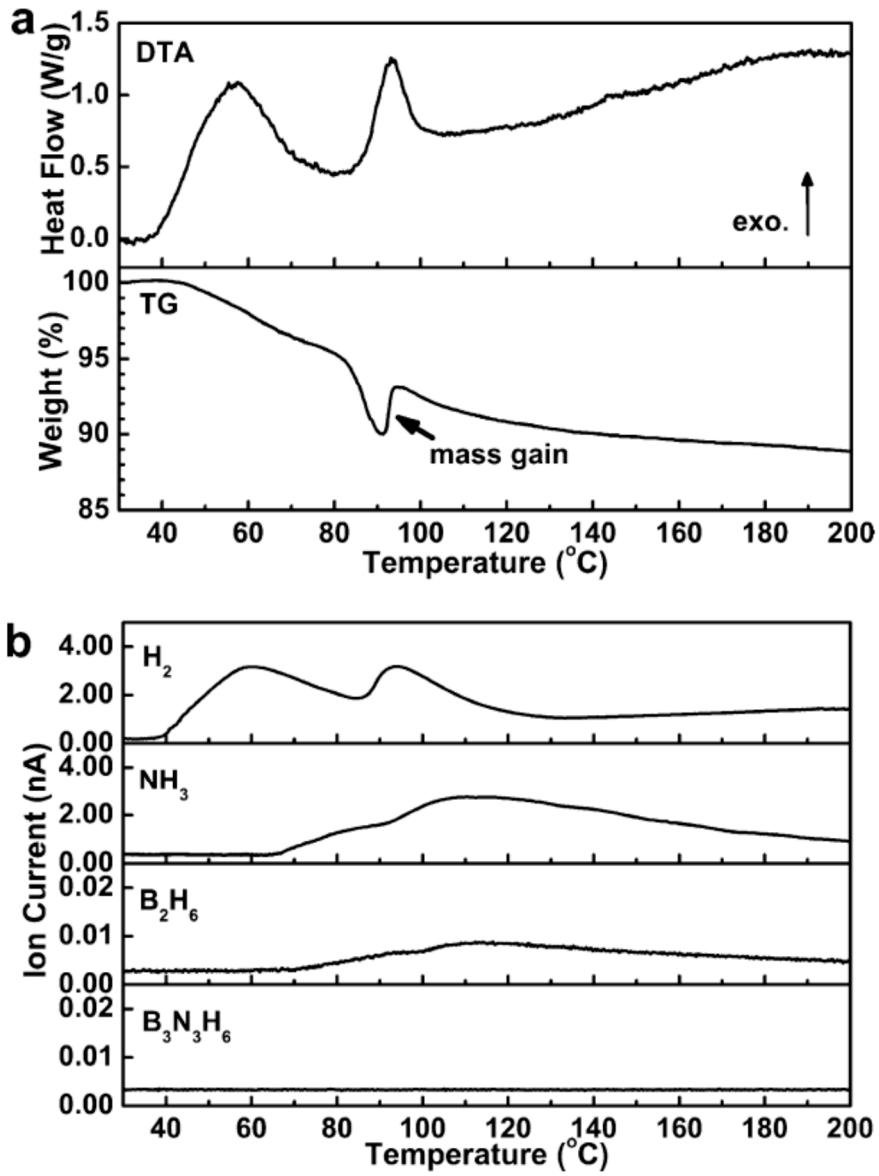

Figure 2. Simultaneous DTA/TG (**a**) and MS (**b**) analysis of the released gas during the reactions of the postmilled SrH_2+2NH_3BH_3 mixture at a heating rate of 2 °C min^{-1}. The mass gain in the TG curve is possibly attributed to some products or intermediates that are formed by the side reaction involving the released H_2 and NH_3 present in the sample environment.

S18. Thermal Decomposition of $Sr(AB)_2$ according to:

[33] Zhang, Q.; Tang, C.; Fang, C.; Fang, F.; Sun, D.; Ouyang, L.; Zhu, M. Synthesis, Crystal Structure, and Thermal Decomposition of Strontium Amidoborane. *J. Phys. Chem. C* **2010**, *114*, 1709.

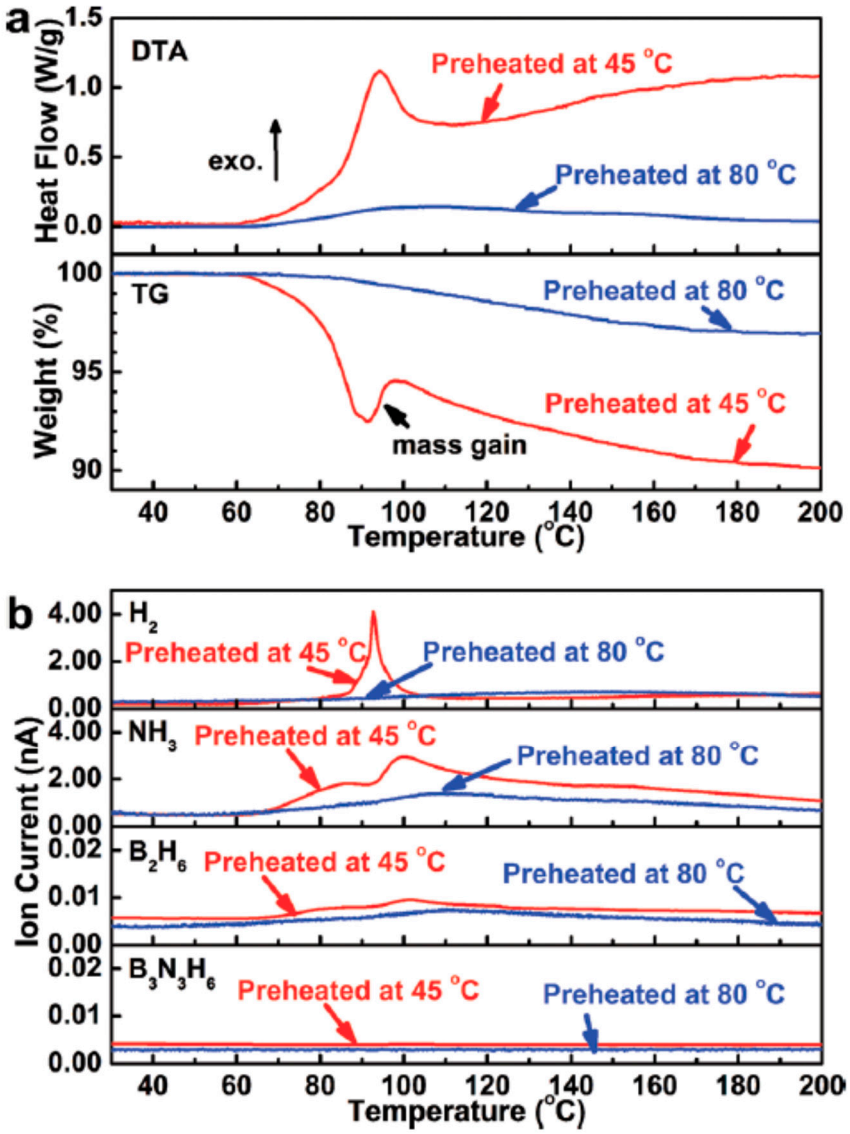

Figure 6. Simultaneous DTA/TG (**a**) and MS (**b**) analyses of the released gases from the samples obtained after gas release of the postmilled SrH_2 + $2NH_3BH_3$ mixture at 45 °C (**red**) and 80 °C (**blue**) for 2 h, respectively. The mass gain in the TG curve is possibly attributed to some products or intermediates that are formed by the side reaction involving the released H_2 and NH_3 present in the sample environment.

S19. Thermal decomposition of $Sr(AB)_2$ according to:

[34] Owarzany, R. Synthesis and Characterization of Zinc Amidoborane. B.Sc. Thesis, University of Warsaw, Warsaw, Poland, 2013.

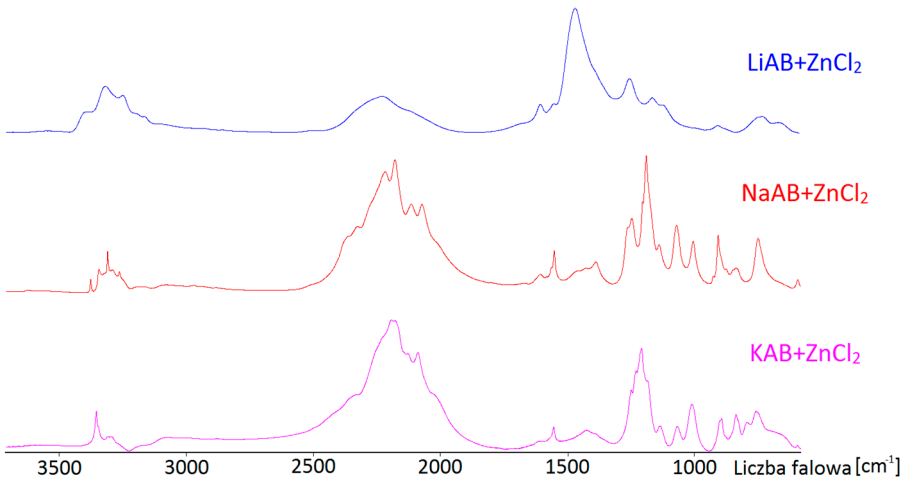

Figure 14. FTIR spectra of products of mechanochemical methatetic reaction at low temperature, reaction substrate were $ZnCl_2$ and (from above): $LiNH_2BH_3$, $NaNH_2BH_3$, KNH_2BH_3.

Adapted with permission from Reference 34 with permission from Rafal Owarzany.

S20. Thermal Decomposition of $Al(AB)_3$ according to:

[35] Hawthorne, M.F.; Jalisatgi, S.S.; Safronov, A.V.; Lee, H.B.; Wu, J. Chemical Hydrogen Storage Using Polyhedral Borane Anions and Aluminum-Ammonia-Borane Complexes, Final Report, University of Missouri, 2010. Available online: http://www.osti.gov/scitech//servlets/purl/990217-xUxbgx/ (accessed on 20 April 2016).

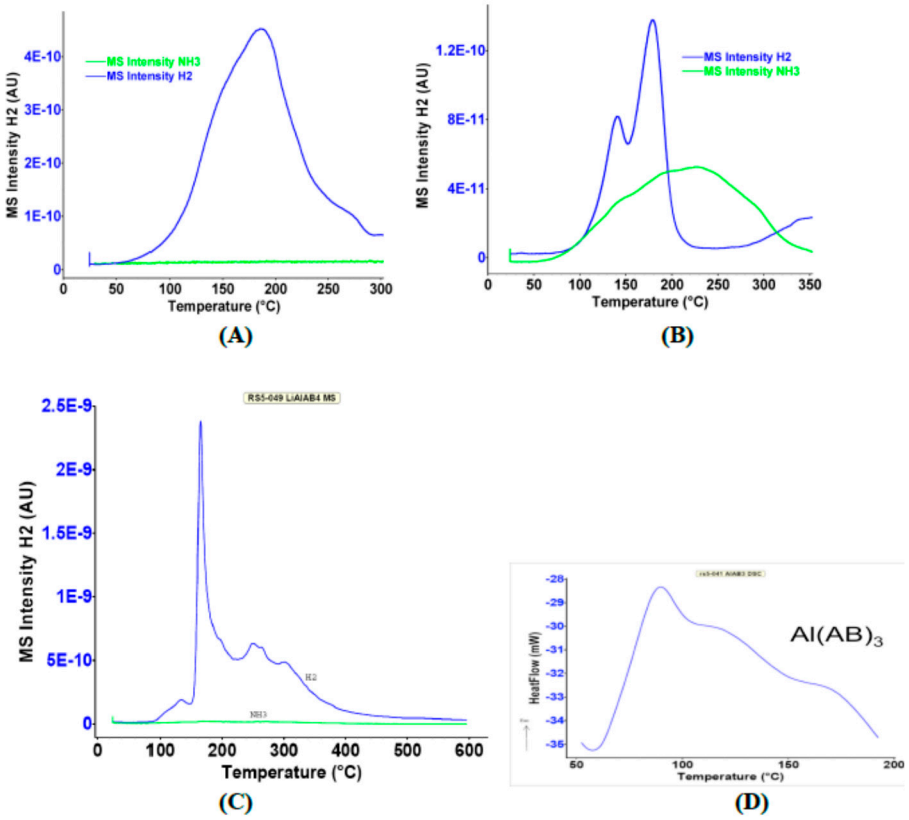

Figure 9. TGA-MS and DSC of Al-AB complexes; (**A**) $Al(AB)_3$; (**B**) Ammonium adduct of $Al(AB)_3$; (**C**) $LiAl(AB)_4$; (**D**) DSC of $Al(AB)_3$.

Spectra of $Al(AB)_3$ reproduced from Reference 36 with permission of M. Frederick Hawthorne.

S21. Thermal Decomposition of $Y(AB)_3$ according to:

[38] Genova, R.V.; Fijalkowski, K.J.; Budzianowski, A.; Grochala, W. Towards Y(NH2BH3)3: Probing hydrogen storage properties of YX_3/MNH_2BH_3 (X = F, Cl; M= Li, Na) and $YH_{x\sim3}/NH_3BH_3$ composites. *J. Alloys Comp.* **2010**, *499*, 144.

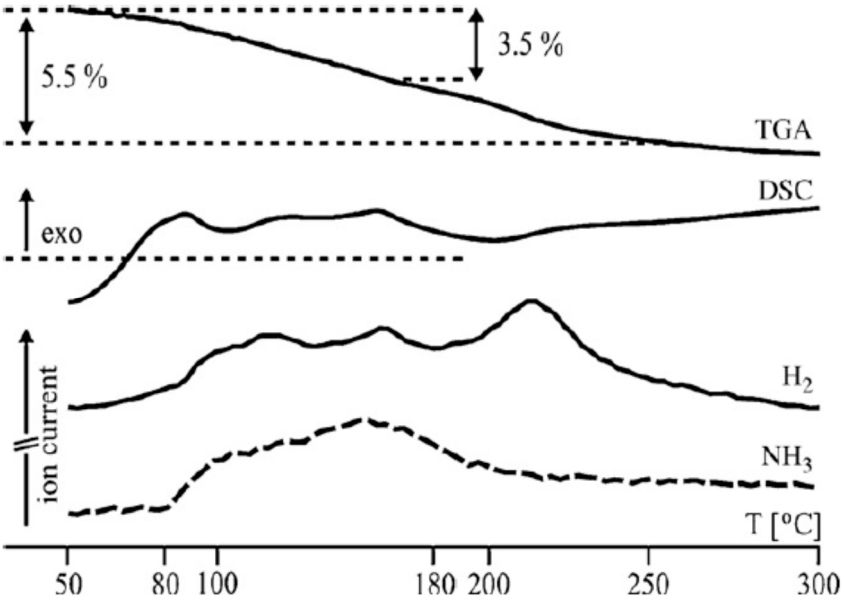

Figure 3. Thermal decomposition of post-milled $YCl_3/LiNH_2BH_3$ composite at 10 K·min^{-1}: TGA and DSC profiles (**top**), H_2 and NH_3 ion currents (**bottom**).

Spectra of $Y(AB)_3$ reproduced from Reference 38 with permission from Elsevier.

S22. Thermal Decomposition of $Y(AB)_3$ according to:

[38] Genova, R.V.; Fijalkowski, K.J.; Budzianowski, A.; Grochala, W. Towards Y(NH2BH3)3: Probing hydrogen storage properties of YX_3/MNH_2BH_3 (X = F, Cl; M= Li, Na) and $YH_{x\sim3}/NH_3BH_3$ composites. *J. Alloys Comp.* **2010**, *499*, 144.

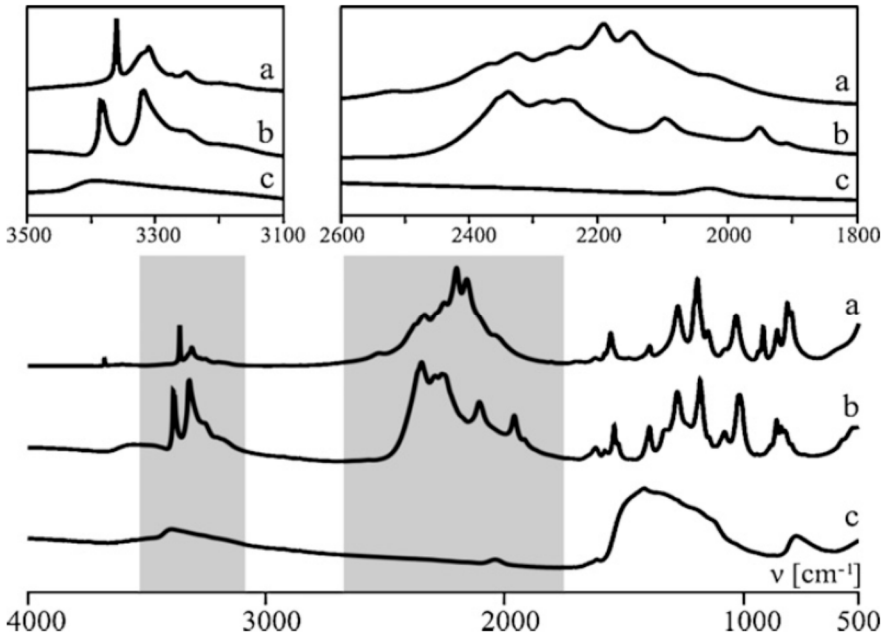

Figure 4. Bottom: FT-IR spectra for (**a**) mixture of the substrates; and for post-milled $YCl_3/LiNH_2BH_3$ composite (**b**) at 20 °C; (**c**) decomposed at 300 °C. **Top**: Focus on BH and NH stretching regions.

Spectra of $Y(AB)_3$ reproduced from Reference 38 with permission from Elsevier.

S23. FTIR spectra of $LiNa(AB)_2$ according to:

[39] Fijalkowski, K.J.; Genova, R.V.; Filnchuk, Y.; Budzianowski, A.; Derzsi, M.; Jaron, T.; Leszczynski, P.J.; Grochala, W. $Na[Li(NH_2BH_3)_2]$—The first mixed-cation amidoborane with unusual crystal structure. *Dalton Trans.* **2010**, *40*, 4407.

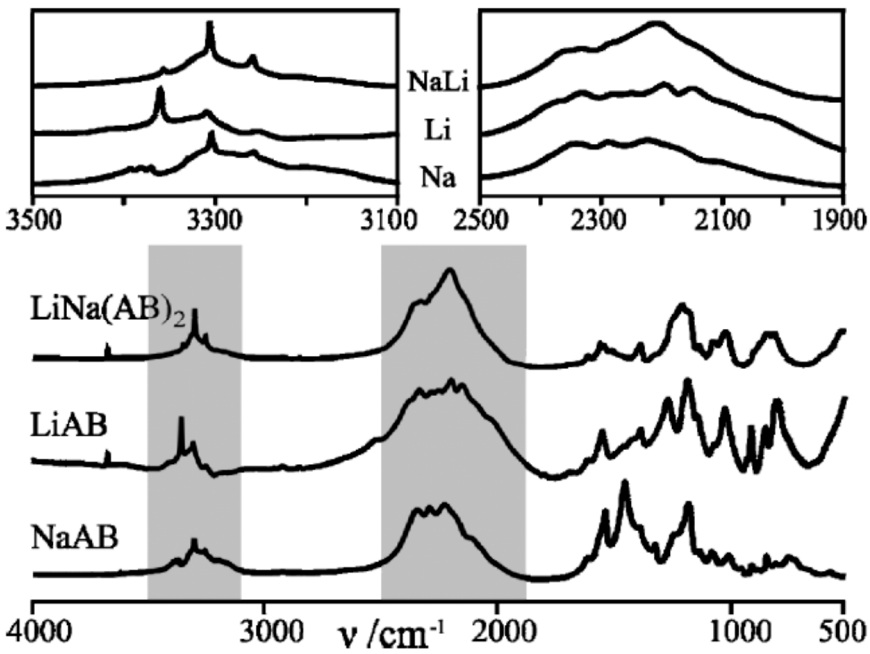

Figure 4. Comparison of the FTIR spectra of $LiNa(AB)_2$ and of the constituent single-cation amidoboranes of lithium and sodium. The ranges marked in grey are shown magnified at the top.

Reproduced from Reference 39 with permission from The Royal Society of Chemistry.

S24. Thermal decomposition of $LiNa(AB)_2$ according to:

[39] Fijalkowski, K.J.; Genova, R.V.; Filnchuk, Y.; Budzianowski, A.; Derzsi, M.; Jaron, T.; Leszczynski, P.J.; Grochala, W. $Na[Li(NH_2BH_3)_2]$—The first mixed-cation amidoborane with unusual crystal structure. *Dalton Trans.* **2010**, *40*, 4407.

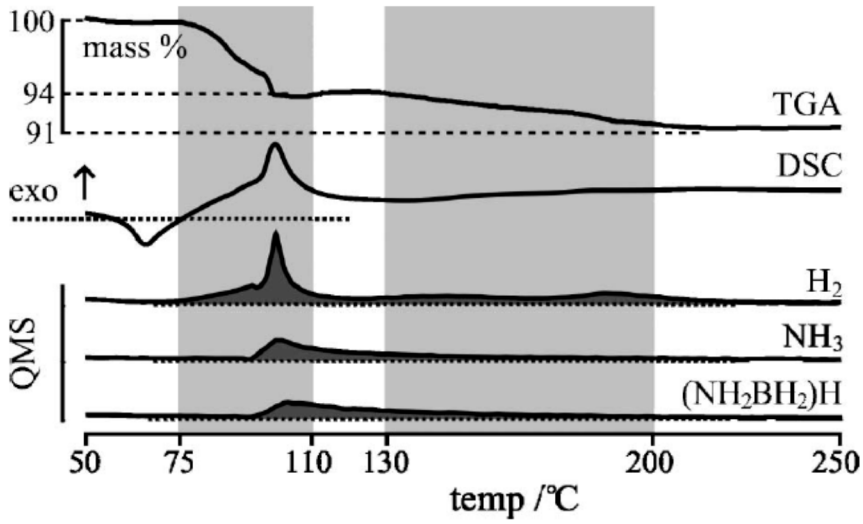

Figure 5. Thermal decomposition of $LiNa(AB)_2$ at 10 K·min^{-1}: TGA and DSC profile (**top**); H_2 NH_3, and NH_2BH_3 ion current (**bottom**). The temperature range shown was cropped to 50–250 °C for better exposition of data. The first and second broad steps of decomposition are marked with gray fields. Note that absolute intensities of MS signals are not directly proportional to the amount of H_2 and N-impurities due to different ionization cross-sections of various molecules for the 40 eV electron beam.

Reproduced from Reference 39 with permission from The Royal Society of Chemistry.

S25. FTIR spectra of $LiAl(AB)_4$ according to:

[40] Xia, G.; Tan, Y.; Chen, X.; Guo, Z.; Liu, H.; Yu, X. Mixed-metal (Li, Al) amidoborane: synthesis and enhanced hydrogen storage properties. *J. Mater. Chem. A* **2013**, *1*, 1810.

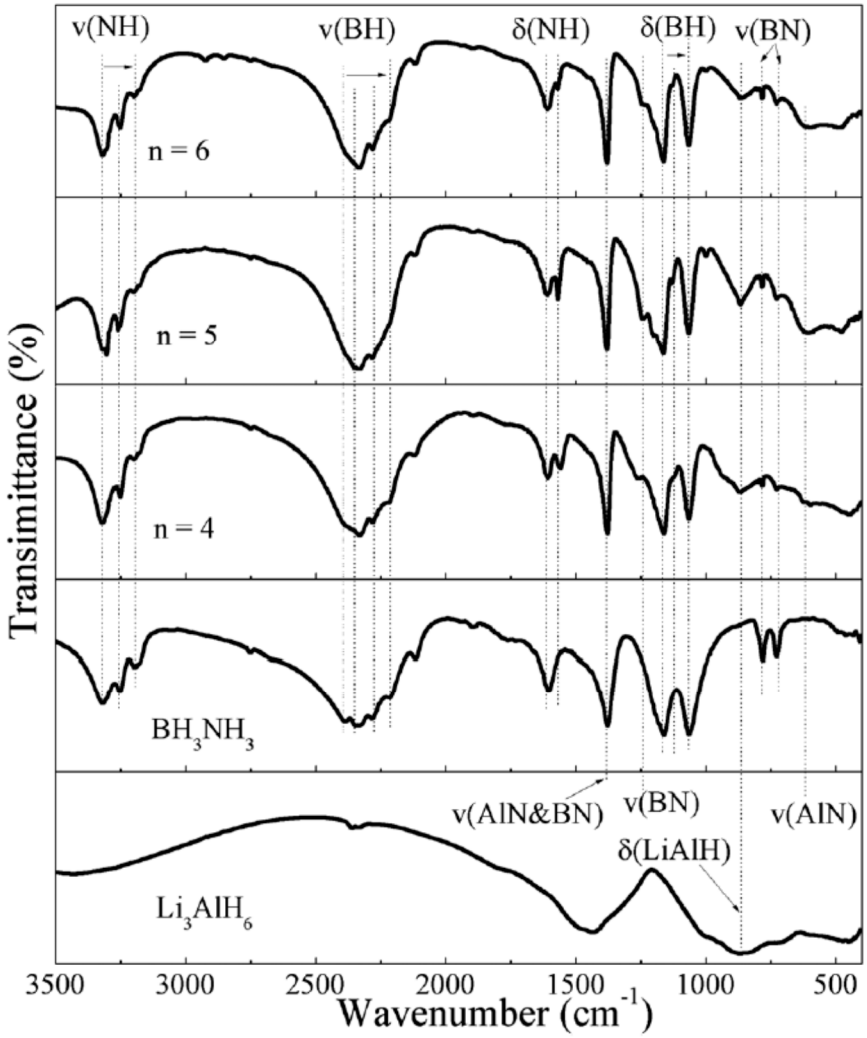

Figure 3. FTIR spectra of the as-prepared Li_3AlH_6–nAB (*n* = 4, 5, and 6) composites, including spectra of pristine AB and as-prepared Li_3AlH_6 for comparison.

Reproduced from Reference 40 with permission from The Royal Society of Chemistry.

S26. Thermal decomposition of LiAl(AB)$_4$ according to:

[40] Xia, G.; Tan, Y.; Chen, X.; Guo, Z.; Liu, H.; Yu, X. Mixed-metal (Li, Al) amidoborane: synthesis and enhanced hydrogen storage properties. *J. Mater. Chem. A* **2013**, *1*, 1810.

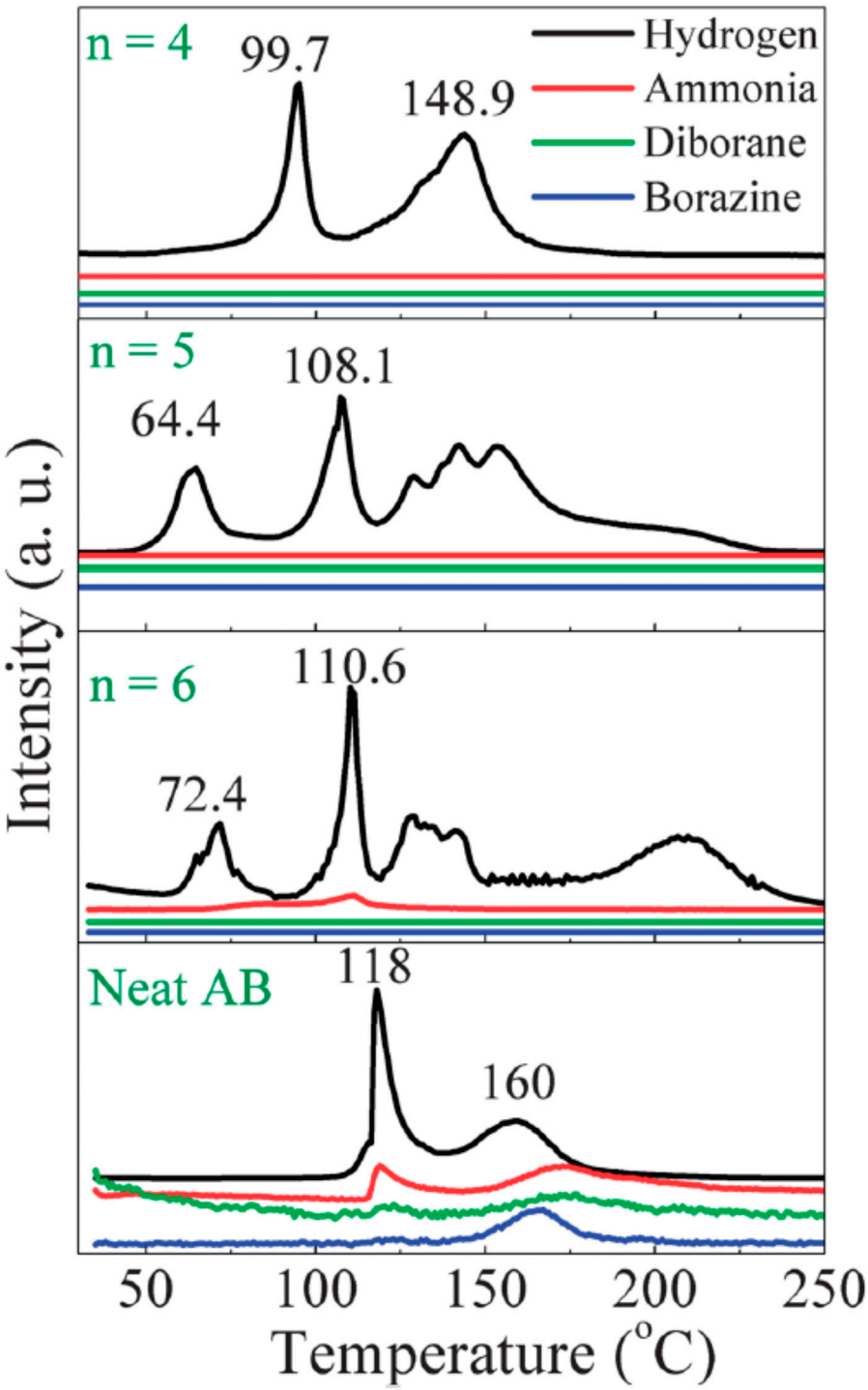

Figure 4. MS spectra of the as-prepared Li_3AlH_6–nAB (n = 4, 5, and 6) composites with a heating rate of 2 °C·min^{-1} under 1 atm dynamic N_2 atmosphere, including neat AB for comparison.

Reproduced from Reference 40 with permission from The Royal Society of Chemistry.

S27. FTIR spectra of $NaAl(AB)_4$ according to:

[41] Dovgaliuk, I.; Jepsen, L.H.; Safin, D.A.; Łodziana, Z.; Dyadkin, V.; Jensen, T.R.; Devillers, M.; Filinchuk, Y. A Composite of Complex and Chemical Hydrides Yields the First Al-Based Amidoborane with Improved Hydrogen Storage Properties. *Chem. Eur. J.* **2015**, *21*, 14562.

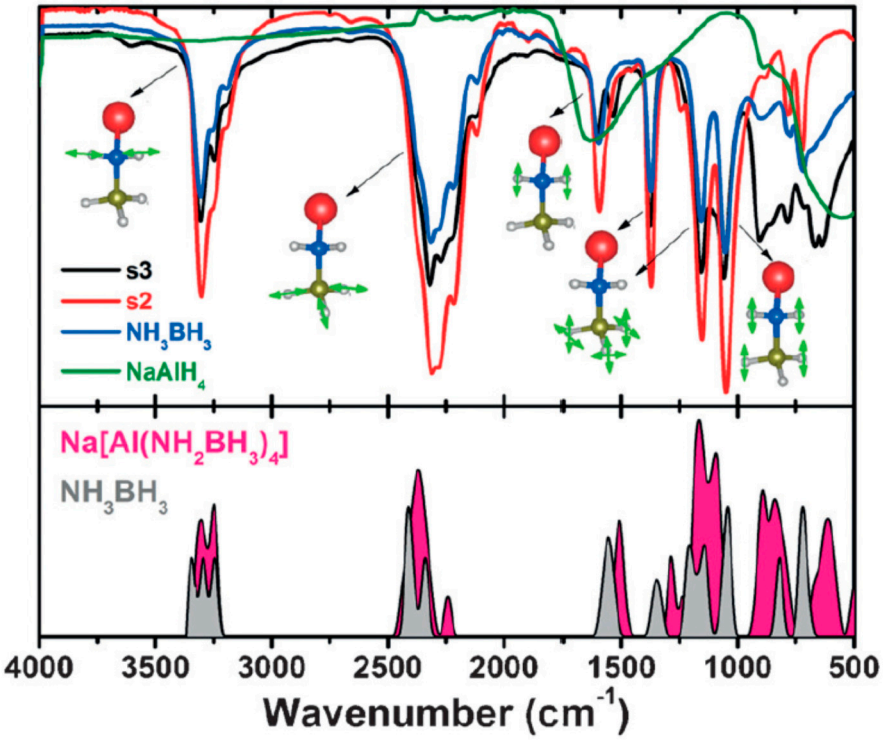

Figure 4. FTIR spectra of the mixtures s2 and s3 (**top**). The spectra of NH_3BH_3 and $NaAlH_4$ are given for comparison. The bottom panel shows the phonon spectra of $Na[Al(NH_2BH_3)_4]$ and NH_3BH_3.

Reproduced from Reference 41 with permission from John Wiley and Sons.

S28. Thermal decomposition of NaAl(AB)$_4$ according to:

[41] Dovgaliuk, I.; Jepsen, L.H.; Safin, D.A.; Łodziana, Z.; Dyadkin, V.; Jensen, T.R.; Devillers, M.; Filinchuk, Y. A Composite of Complex and Chemical Hydrides Yields the First Al-Based Amidoborane with Improved Hydrogen Storage Properties. *Chem. Eur. J.* **2015**, *21*, 14562.

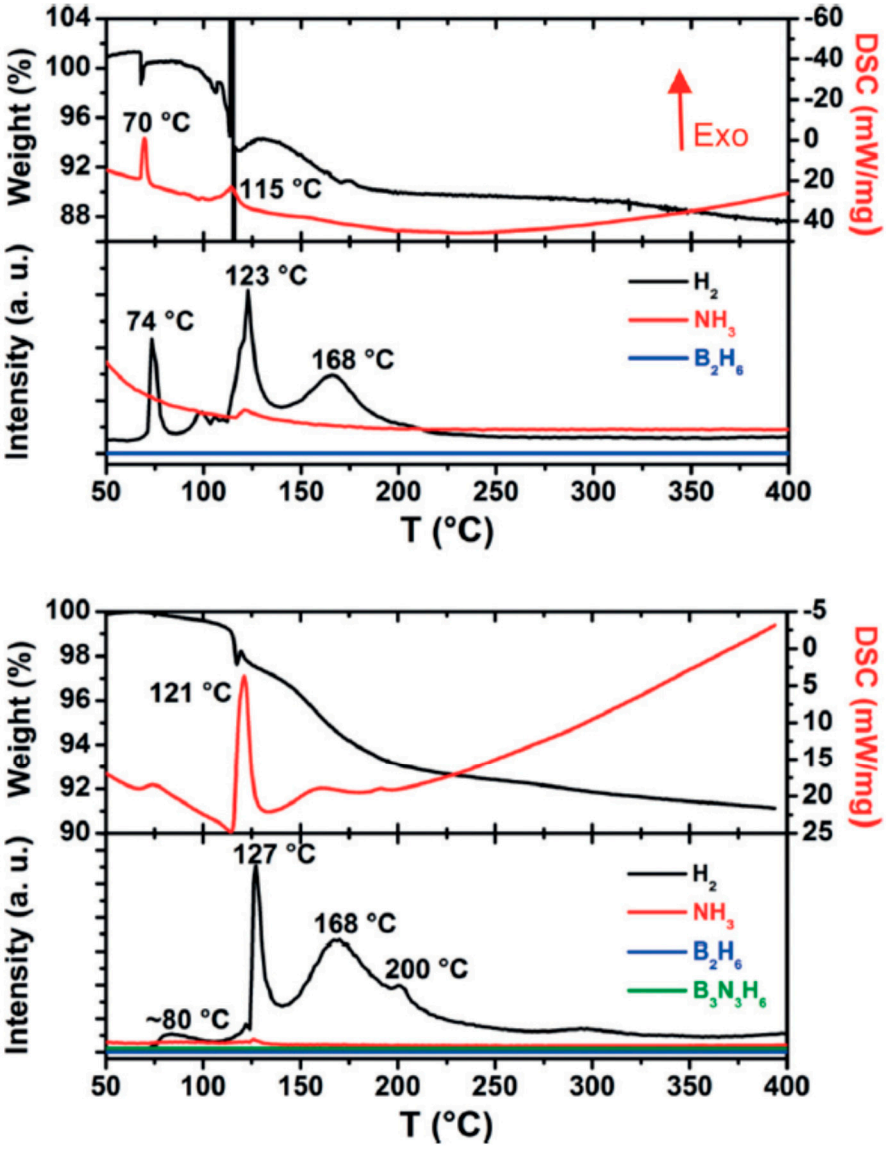

Figure 6. TGA–DSC–MS analyses for s2 (**top**) and s3 (**bottom**) performed under a dynamic argon atmosphere.

Reproduced from Reference 41 with permission from John Wiley and Sons.

S29. Thermal Decomposition of $NaMg(AB)_3$ according to:

[42] Kang, X.; Luo, J.; Zhang, Q.; Wang, P. Combined formation and decomposition of dual-metal amidoborane $NaMg(NH_2BH_3)_3$ for high-performance hydrogen storage. *Dalton Trans.* **2011**, *40*, 3799.

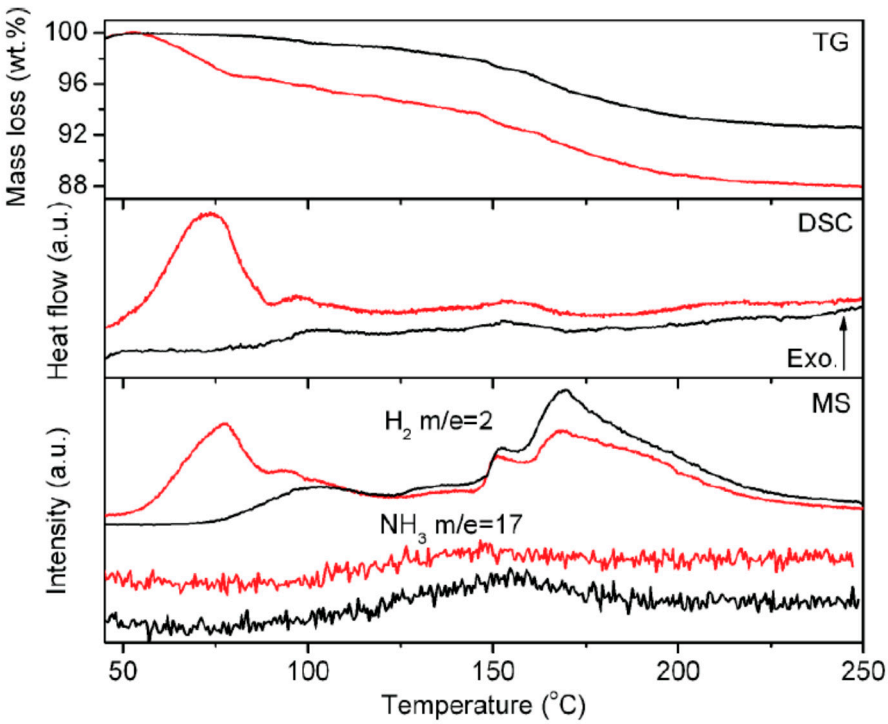

Figure 3. TG/DSC/MS profiles of the $3AB/NaMgH_3$ samples: post-milled (red lines) and post-treated at 45 °C (black lines). The ramping rate is 2 °C·min^{-1}.

Reproduced from Reference 42 with permission from The Royal Society of Chemistry.

S30. Thermal Decomposition of $Na_2Mg(AB)_4$ according to:

[44] Wu, H.; Zhou, W.; Pinkerton, F.E.; Meyer, M.S.; Yao, Q.; Gadipelli, S.; Udovic, T.J.; Yildirim, T.; Rush, J.J. Sodium magnesium amidoborane: The first mixed-metal amidoborane. *Chem. Commun.* **2011**, *47*, 4102.

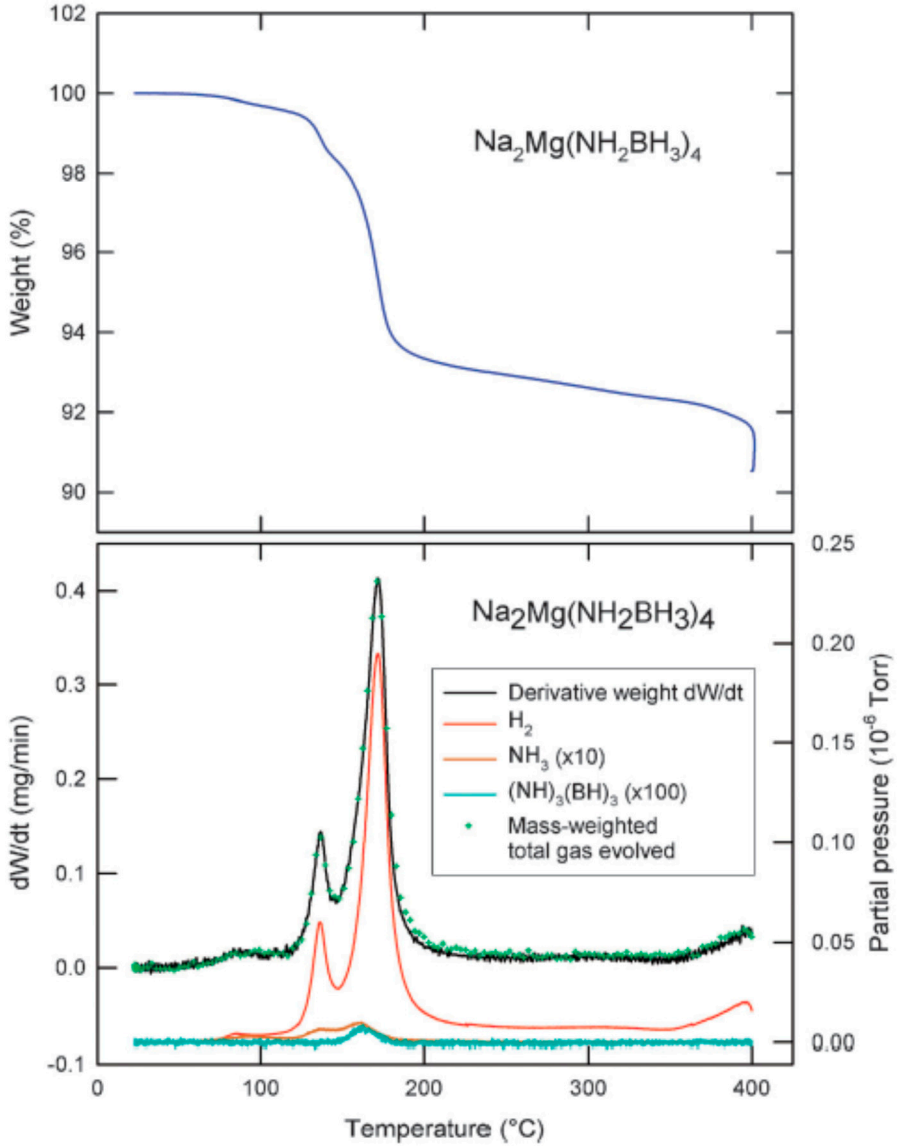

Figure 2. TGA weight loss (**upper panel**) and the accompanying MS partial pressures (**lower panel**) for $Na_2Mg(NH_2BH_3)_4$ measured at 1.7 °C·min^{-1} to 400 °C. The rate of weight loss dW/dt (black curve) is also shown. Note that the NH_3 signal has been multiplied by a factor of 10 and the $(NH)_3(BH)_3$ signal has been multiplied by 100 to be visible on the same scale as H_2. The green crosses are the total mass contribution H_2 + NH_3 + borazine to the evolved gas, scaled to compare with dW/dt.

S31. FTIR Spectra of $Na_2Mg(AB)_4$ and $K_2Mg(AB)_4$ according to:

[45] Chua, Y.S.; Li, W.; Wu, G.; Xiong, Z.; Chen, P. From Exothermic to Endothermic Dehydrogenation—Interaction of Monoammoniate of Magnesium Amidoborane and Metal Hydrides. *Chem. Mater.* **2012**, *24*, 3574.

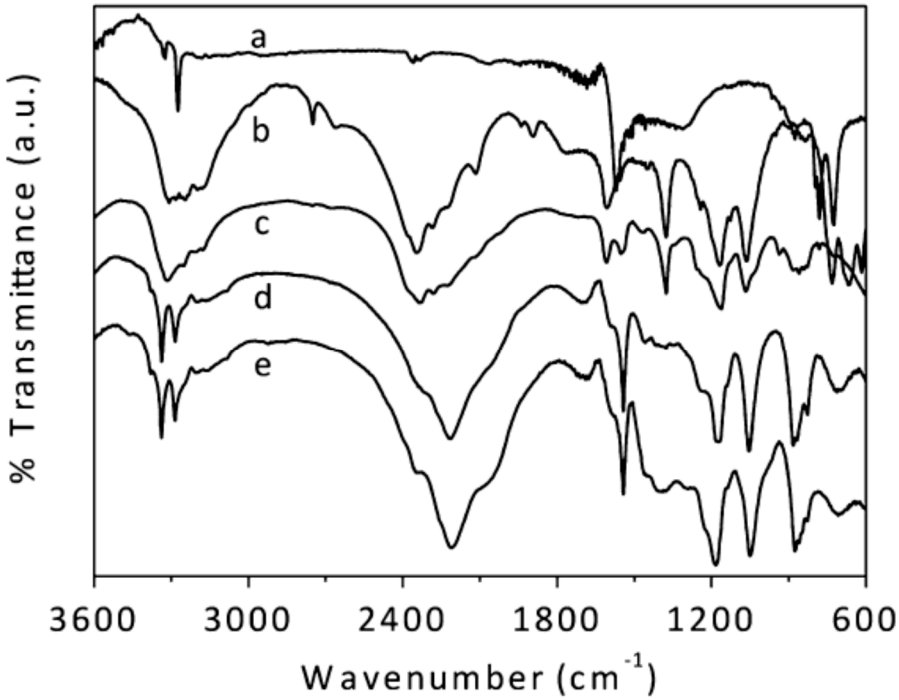

Figure 2. FTIR spectra of (**a**) $Mg(NH_2)_2$; (**b**) AB; (**c**) $Mg(NH_2BH_3)_2{\cdot}NH_3$; (**d**) postmilled $Mg(NH_2BH_3)_2{\cdot}NH_3$+KH sample; and (**e**) the postmilled $Mg(NH_2BH_3)_2{\cdot}NH_3$+NaH sample.

S32. Thermal Decomposition of $Na_2Mg(AB)_4$ and $K_2Mg(AB)_4$ according to:

[45] Chua, Y.S.; Li, W.; Wu, G.; Xiong, Z.; Chen, P. From Exothermic to Endothermic Dehydrogenation—Interaction of Monoammoniate of Magnesium Amidoborane and Metal Hydrides. *Chem. Mater.* **2012**, *24*, 3574.

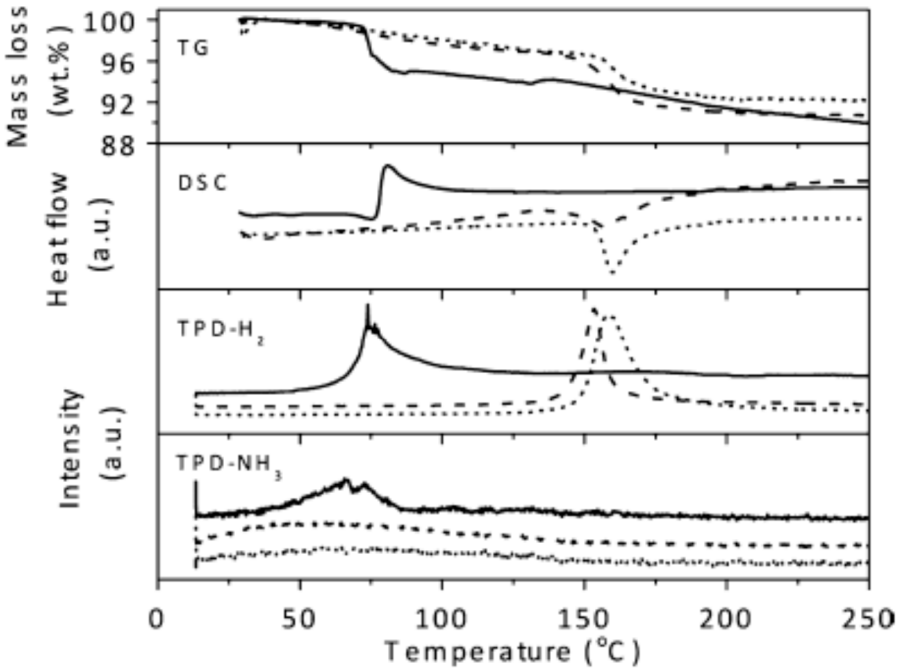

Figure 5. Comparison of the TG-DSC and TPD−MS curves of $Mg(NH_2BH_3)_2{\cdot}NH_3$ (solid line), $Na_2Mg(NH_2BH_3)_4$+$Mg(NH_2)_2$ (dashed line), and $K_2Mg(NH_2BH_3)_4$+$Mg(NH_2)_2$ (dotted line) composites. The temperature was ramped at 2 °C/min.

Reprinted with permission from Chua Y.S. *Chem. Mater.* 2012, *24*, 3574. Copyright 2012 American Chemical Society.